Received 8 August 2023; revised 16 October 2023; accepted 29 October 2023. Date of publication 17 November 2023; date of current version 30 January 2024.

Digital Object Identifier 10.1109/OJAP.2023.3333900

A Compact, Circularly-Polarized, Substrate-Integrated Waveguide, Millimeter-Wave Beamsteering System for 5G Mobile Terminals

KHALED AL-AMOODI [1] (Member, IEEE), RASHID MIRZAVAND [1] (Senior Member, IEEE), MOHAMMAD MAHDI HONARI [2] (Senior Member, IEEE), JORDAN MELZER [3] (Member, IEEE), DUNCAN G. ELLIOTT [1] (Senior Member, IEEE), AND PEDRAM MOUSAVI [4] (Senior Member, IEEE)

[1]Department of Electrical and Computer Engineering, University of Alberta, Edmonton, AB T6G 1H9, Canada
[2]Kymeta Corporation, Redmond, WA 98052, USA
[3]Department of Technology Strategy, TELUS Communications, Ottawa, ON K1P 0A6, Canada
[4](Deceased) Department of Electrical and Computer Engineering, University of Alberta, Edmonton, AB T6G 1H9, Canada

CORRESPONDING AUTHOR: R. MIRZAVAND (e-mail: mirzavan@ualberta.ca)

This work was supported in part by the Natural Sciences and Engineering Research Council (NSERC); in part by CMC Microsystems; in part by Alberta Innovates; and in part by TELUS Communications.

ABSTRACT A compact, circularly-polarized (CP), end-fire, 4×1 continuous beamsteering antenna array implemented using substrate-integrated waveguides for 5G mobile terminals is proposed in this paper. The purpose of this system is to complement the radiation patterns of planar phased arrays on the faces of a typical mobile terminal. The proposed system seamlessly integrates previously-presented antennas and polarizers, with adjustable phase shifters and a feeding network in a multi-layered, single stack, printed circuit board (PCB) for continuous beamsteering in a compact package. Through the use of forward and reverse couplers, and the stacking of the phase shifters on top of the feeding network, a compact form factor of $7.6 \times 4.1 \times 0.38\lambda_o^3$ is achieved. The system was fabricated and assembled through standard PCB processes. The measurements illustrated that the system can achieve a continuous beamsteering range of $\pm 35^\circ$ with an axial ratio better than 3 dB and a gain variation less than 3 dB. A measured impedance bandwidth (BW) of 8.9% at 28 GHz is also demonstrated. Given its performance, size, ease of manufacture, integrated control lines and single RF feed, the proposed system is a good candidate for 5G millimeter-wave continuous beamsteering in mobile terminals.

INDEX TERMS 5G, antenna arrays, beamsteering, circular polarization, compact, end-fire, fifth generation, millimeter-wave, mobile device, mobile terminal, reflection-type phase shifter, substrate-integrated waveguide.

I. INTRODUCTION

IN ORDER to better meet the ever-growing demand for faster handheld mobile communication, several major core technologies have been proposed for the fifth generation of cellular communication (5G) [1]. One of those solutions is the use of wide spectrum available in millimeter-wave (mmWave) frequencies [2], [3], [4], [5], such as the 850 MHz free band at 28 GHz [6]. At those higher frequencies, beamsteering antenna arrays are used so as to compensate for unavoidably-high path loss (due to smaller antenna apertures) [7]. One of the major benefits of beamsteering is that it provides greater user coverage through less spatial interference with other users. Further improvement in performance can be achieved in 5G systems through the use of circularly-polarized (CP) antennas as they reduce multipath interference, enable polarization diversity and eliminate polarization mismatch loss (for same polarization rotation sense) [8], [9].

While large beamsteering mmWave CP systems are not difficult to implement at base stations, such solutions in

mobile terminals present several limitations including power, space, compatibility with standard printed circuit board (PCB) processes, and detrimental effects of the user's hand and head on the radiation. Compatibility with standard PCB processes can be achieved through designing a fully substrate-integrated waveguide (SIW) system, with benefits such as easy manufacturing and low loss [10], [11], [12], [13], [14]. To mitigate the effects of the user on radiation patterns, one solution can be to place antenna arrays, with end-fire radiation pattern, on the edges of a mobile terminal [15], [16]. These arrays can be used alongside planar antenna arrays to ensure spherical coverage around a mobile terminal.

Recently, many end-fire arrays for use in 5G mobile applications have been presented [17], [18], [19], [20]. Unfortunately, these arrays do not incorporate a beamsteering mechanism and thus cannot be implemented in mobile terminals yet. These arrays are in contrast to surface-emitting arrays (such as that presented in [14], which is additionally also not CP and also does not demonstrate continuous beamsteering capabilities). There are, however, several beamsteering arrays that share some or all of this paper's goals (compact form factor, circular polarization and continuous beamsteering) [21], [22], [23], [24], [25], [26]. Specifically, we consider a system to be compact if its length and width are $\leq 10\lambda$, and its height is $\leq 0.5\lambda$. While the beamsteering array in [26] is composed of a compact SIW structure, it does not lend for easy integration due to the need of screws/mounts, the use of active devices on both sides of the board, and the lack of an integrated biasing network (or control lines). In addition, the antennas are linearly-polarized (LP), thereby limiting their applications in 5G mobile terminals. Finally, while it is presented as a 5G system, it is a misnomer as it is a 5 GHz WiFi system, thus it may not scale well to mmWave frequencies especially when considering the phase shifters. The array in [25] achieves compactness through the use of switches to adjust passive elements in the vicinity of the active antenna element. However, it demonstrates a really wide azimuth beamwidth and limited pre-defined beam-directions which will result in interference with nearby users. Furthermore, an actual switching mechanism has not been demonstrated. Finally, the antennas are LP and it is unclear if the system will translate well to arrays with circular polarization. The designs in [21], [22], [23], [24] present beamsteering arrays with identical feeding and phase shifting networks. From these works, only the designs in [22] and [24] are CP end-fire systems, yet they only have fixed pre-defined beam directions and also lack a mechanism for beam switching. It is therefore tough to integrate them within mobile terminals in their current state.

This paper will present a compact end-fire 4×1 beam-steering system with circular polarization in SIW, for the purpose of enabling 5G mmWave communication in mobile terminals. This builds upon our work in [20], [27], by introducing continuous beamsteering in a compact package, whereas previously we only demonstrated arrays with fixed beam directions, hardwired in the PCBs for demonstration only. The technical challenges to designing and fabricating such a system are two-fold: how does one fit the beam-steering and circular polarization capabilities within a small package, and how does one ensure that the proposed design can be consistently manufactured and easily integrated within a mobile terminal. The contribution and features of this paper are as follows:

- Multi-layered system architecture with a volume of only $11.8\lambda_o^3$ using forward and reverse couplers.
- Proposing a monolithic system architecture in standard PCB technology for repeatable fabricated performance similar to simulations, and for ease of integration in mobile terminals.
- Continuous beamsteering range of $\pm 35°$ with circular polarization axial ratio and gain variation of ≤ 3 dB.
- Having a bandwidth (BW) of 8.9% at 28 GHz - appropriate for the FCC-allocated n261 band (27.5 to 28.35 GHz).

The proposed system architecture is presented in Section II. In Section III, the blocks of the system, including the phase shifter, feeding network, antennas, and polarizers, are demonstrated. Measurement results are presented in Section IV, alongside a comparison with other designs. Finally, conclusions are provided in Section V.

II. BEAMSTEERING SYSTEM ARCHITECTURE

While beamsteering with circular polarization is not as complex to achieve on the faces of a standard mobile terminal, the same cannot be said for beamsteering from a terminal's edges. In order to address the resulting lack in beam coverage, the proposed architecture must meet several key requirements:

- Circular polarization
- Compact
- Continuous steering
- Edge-radiating
- Integrated control lines
- Manufacturable in standard PCB processes
- mmWave
- Single RF feed

Based on the requirements above, we propose a compact SIW, CP, edge-radiating 4×1 beamsteering system that is designed in a stack of three substrates of RO4350B with thicknesses of 0.5 mm (substrate 1), 1.8 mm (substrate 2) and 1.8 mm (substrate 3), with metal layers in between, for a total thickness of 4.1 mm. A block diagram of the proposed system is shown in Fig. 1, with enclosing boxes depicting which substrate layers each block is implemented in. The structure consists of one 1-to-4 power splitter with a transition from grounded coplanar waveguide (GCPW) to SIW in substrate 2, four reverse couplers from substrate 2 to substrate 1, four reflection-type phase shifters (RTPSs) in substrate 1, four forward couplers from substrate 1 to

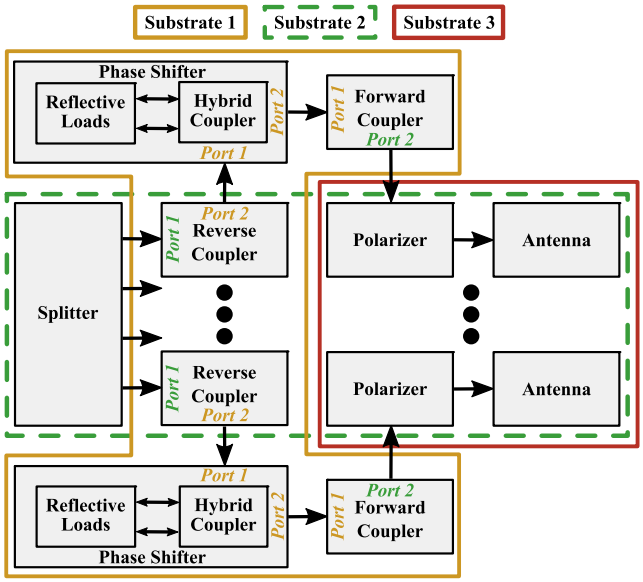

FIGURE 1. Block diagram of the proposed end-fire, CP, SIW 4 × 1 beamsteering system, with the occupied substrate layers of each block shown.

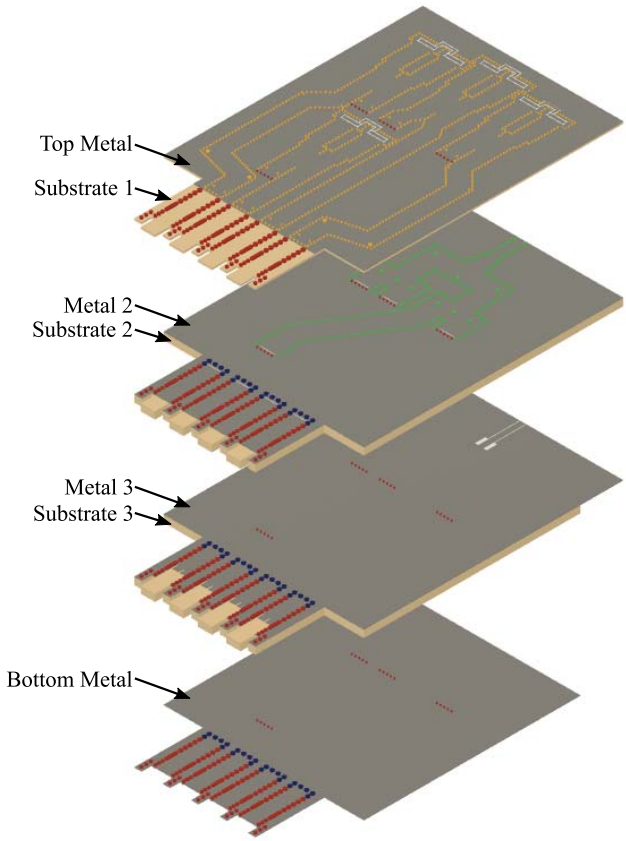

FIGURE 2. Exploded view of the proposed end-fire, CP, SIW 4 × 1 beamsteering system.

substrate 2, four polarizers in substrates 2 and 3, and four radiating elements in substrates 2 and 3. An exploded view of the beamsteering system is shown in Fig. 2, illustrating how the different blocks shown Fig. 1 are stacked and arranged. The four radiating elements are spaced with a pitch of $0.67\lambda_o$ (7.2 mm at 28 GHz, where λ_o is 10.7 mm), to reduce coupling between elements, at the expense of grating lobes appearing at large steering angles. Sections of SIWs are also included between the splitter and RTPSs, and between the RTPSs and polarizers to ensure equal delays for all four antennas despite the positioning of the phase shifters. The beamsteering system is designed with PCB limitations such as via sizes, annular rings and adhesive layers in mind, and is thus manufacturable without the need of screws to combine the layers together. This also ensures repeatability and closeness of measurements to simulations.

III. SUPPORTING SYSTEM BLOCKS

While the overall architecture is the novelty of this paper, the individual blocks in the beamsteering CP system must be properly designed and characterized. To ensure that the system is monolithic and fully integrated, all blocks are designed using the same dielectric: Rogers RO4350B with relative permittivity of 3.66 and loss tangent of 0.0037.

A. PHASE SHIFTER

In a beamsteering array, the ideally required phase shift range is dictated by the incremental phase shifts between elements needed to steer the beam over its pointing range. For an array with element spacing $d = 7.2$ mm, the incremental phase shift is found using the following equation [28]

$$\delta = \frac{360^\circ \cdot d \cdot \sin\theta_s}{\lambda_o} \tag{1}$$

where δ and θ_s are, respectively, the incremental phase shift and intended azimuth beam direction in degrees, and λ_o is the free-space wavelength. Incremental phase shifts of 0°, ±40°, ±80°, ±120°, and ±160° are required for steering up to ±40° with steering steps of 10°. Specifically, for steering to ±20° and ±30°, their respective incremental phase shifts results in a maximum array element phase shift of 240°. Additionally, the phase shifter needs to meet the following requirements: continuous phase control (for continuous steering), low insertion loss (IL) variation with voltage sweep, adequate impedance matching BW, single substrate layer SIW with elements on one side only, integrated biasing circuitry, small size, and low cost. Therefore, a single substrate layer SIW reflection-type phase shifter (RTPS), demonstrated in [29], [30], with a substrate-integrated biasing network for a continuously tunable phase shift of close to 240° is sufficient for ±30° beamsteering, which is the goal of this paper.

The layout of the proposed RTPS is shown in Fig. 3 and its dimensions are listed in Table 1. The RTPS consists of a single substrate layer SIW 3 dB hybrid coupler with two of its adjacent ports being coupled to SIW reflective loads. The reflective loads are designed identically. They

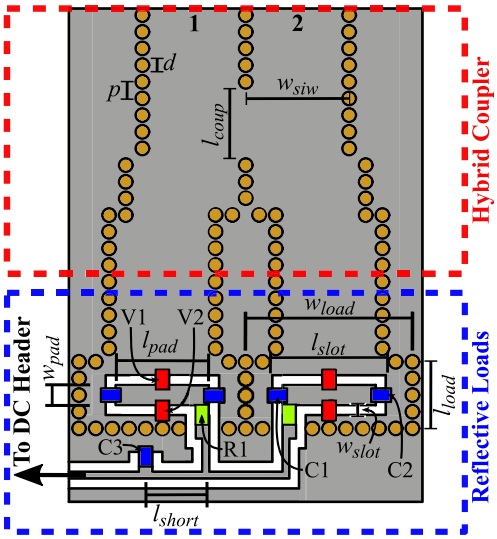

FIGURE 3. Layout of the proposed single substrate layer SIW RTPS with integrated biasing network, where V1 and V2 are varactor diodes, C1 and C2 are DC block capacitors, C3 is an AC short capacitor, and R1 is a resistor. V1, V2, C1, C2 and R1 are present at both reflective loads.

TABLE 1. Dimensions of the proposed single substrate layer SIW RTPS with integrated biasing network.

Parameter	l_{coup}	l_{load}	l_{slot}	l_{pad}	l_{short}	p	d
Value (mm)	6.0	2.4	5.8	3.6	1.9	0.8	0.4
Parameter	w_{siw}	w_{load}	w_{slot}	w_{pad}			
Value (mm)	4.4	6.7	0.15	1.3			

are both wider than the SIW lines that they are coupled to. Varactors for phase shifting are soldered across the slots at the positions shown, with cathodes being connected to the DC island, i.e., the metal patch between the varactors. The same reverse bias voltage is applied at both DC islands and hence four varactors, through the biasing network consisting of capacitors and resistors. In a mobile terminal, the bias lines would be coupled to the appropriate control system if it is implemented on the same substrate stack. In this paper, the DC paths are coupled to headers for easier use with DC power supplies; however, a real-life application in a mobile terminal could see the DC paths coupled to integrated circuits on the same PCB for voltage control, and thus beamsteering.

In order to characterize the proposed SIW RTPS's performance, it is manufactured on a 0.5-mm-thick RO4350B substrate. The reverse bias control voltage, which is equal across all varactors, is swept from 0 V to 16 V with 0.5 V intervals. Fig. 4(a) presents the measured reflection coefficients of the phase shifter as the voltage is swept. An impedance matching BW of >13% at 28 GHz is achieved. Fig. 4(b) demonstrates the achievable measured phase shift range of the phase shifter over frequency. The maximum phase shift is 219° at 28 GHz with a small slope of −0.04°/MHz. For our beamsteering application, it is also important to know what control voltage is required to achieve

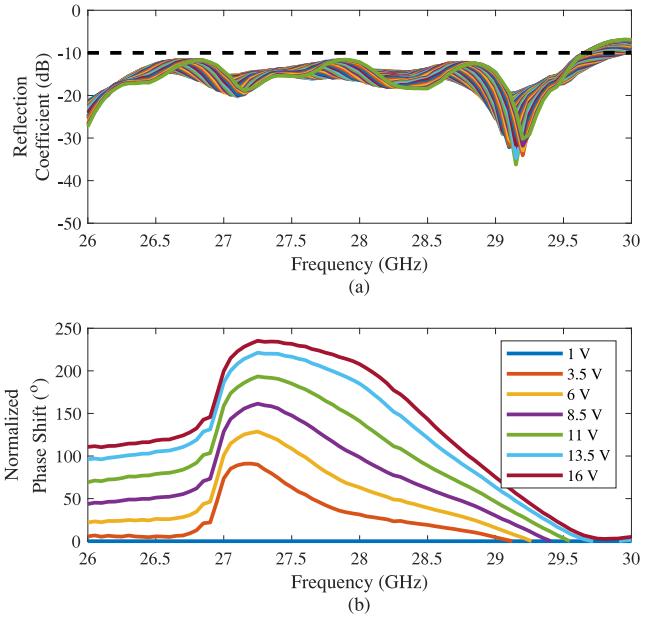

FIGURE 4. Measured performance of the proposed SIW RTPS against frequency. (a) Reflection coefficient for control voltages 0 to 16 V with 0.5 V steps. (b) Phase shift for control voltages 1 to 16 V with 2.5 V steps.

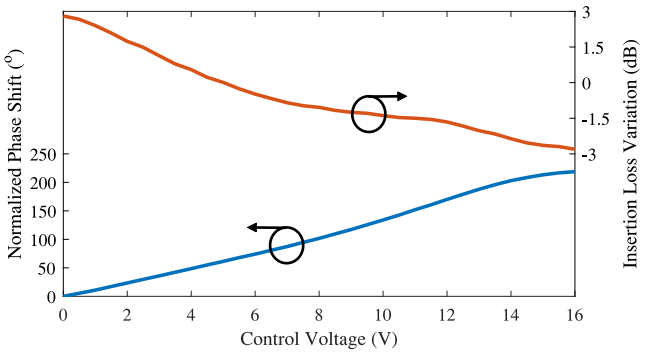

FIGURE 5. Measured phase shift and IL variation of the proposed SIW RTPS with control voltage at 28 GHz.

TABLE 2. Dimensions of the splitter and the GCPW-to-SIW transition for the beamsteering system.

Parameter	l_1	l_2	l_3	w_1	w_2	w_3	w_4	w_5
Value (mm)	2.5	2.6	10.0	2.5	1.4	0.1	0.7	5.3
Parameter	w_6	w_7	s_1	s_2	s_3	s_4	d_1	d_2
Value (mm)	5.4	9.0	2.0	3.5	2.5	7.2	0.4	0.7

a specific phase. Presented in Fig. 5 are the normalized phase shift and IL variation of the phase shifter at 28 GHz versus control voltage.

B. SPLITTER

The next block to consider is the splitter. Given that a 4×1 beamsteering array is being designed, the splitter will be used to split the input power equally with the same phase to four outputs. The 1×4 splitter is implemented on a 1.8-mm-thick multi-layered substrate as two stages of T-junctions

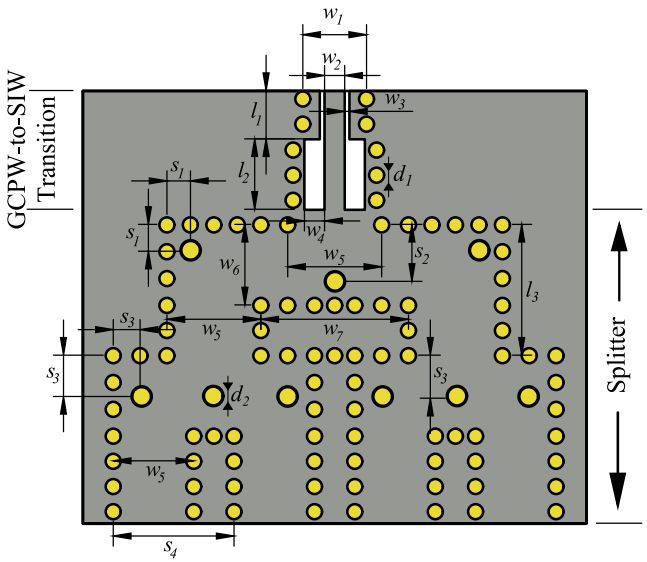

FIGURE 6. Layout of the splitter and the GCPW-to-SIW transition for the beamsteering system.

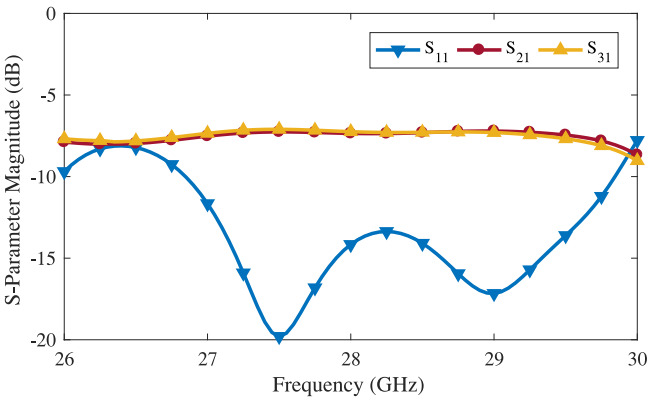

FIGURE 7. Simulated S-Parameter magnitudes of the splitter with the GCPW-to-SIW transition. S_{41} and S_{51} are not included due to symmetry.

and L-bends [31] to accommodate the antennas with the pitch of 7.2 mm. Furthermore, the input will incorporate a GCPW-to-SIW transition to measure the performance of the system. The transition is implemented as wide slots on the metal to match the GCPW impedance of 50 Ω to that of the SIW [32]. The layout of the splitter and GCPW-to-SIW transition is shown in Fig. 6 while the dimensions are provided in Table 2. The simulated results of the splitter with the transition are shown in Fig. 7. The input is port 1 while the outputs plotted are ports 2 and 3. Ports 4 and 5 have similar results to ports 3 and 2, respectively, due to symmetry. The impedance BW is 10.7%. The transmission coefficient is −7.2 dB at all outputs indicating an IL of 1.2 dB due to the transition and SIW splitter.

C. ANTENNA AND POLARIZER

Arguably, the design of the polarizers and antennas is one of the most crucial parts of the beamsteering system as those two components dictate the axial ratio (AR) and

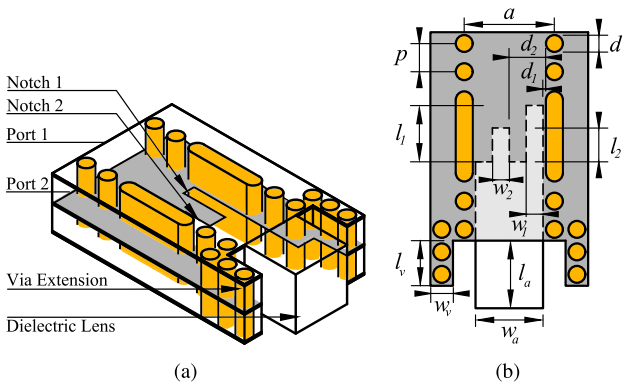

FIGURE 8. Layout of the polarizer and antenna for the beamsteering system [20], [27]. (a) Isometric view. (b) Metal between substrates 2 and 3 are shown.

TABLE 3. Dimensions of the polarizer and antenna [20], [27].

Parameter	a	d	p	d_1	d_2	l_1	l_2
Value (mm)	4.50	1.00	1.20	0.18	2.03	1.45	1.32
Parameter	l_a	l_v	w_1	w_2	w_a	w_v	
Value (mm)	3.60	2.50	0.15	0.30	3.60	1.80	

elevation gain beamwidths, and the maximum azimuth beamsteering range, both in gain and AR. For good coverage, single element azimuth and elevation beamwidths of ±35° are sought. Furthermore, as with the other blocks, the structure needs to be compact. The proposed system will thus incorporate compact SIW notched-septum polarizers and dielectric lens antennas which we have previously demonstrated [20], [27].

The layout of the polarizer and antenna is shown in Fig. 8. An isometric view of substrates 2 and 3 and the metal layer between those substrate layers are shown. Some metal layers are not shown in the isometric views for clarity. Dimensions are provided in Tables 3. Two notches of appropriate dimensions are etched into the metal between substrates 2 and 3 in order to polarize the vertical TE_{10} mode fields from the rectangular SIW input port into TE_{01} mode horizontal and TE_{10} mode vertical fields with 90° phase offset at the square SIW open end, thereby resulting in CP radiation. A cubic dielectric lens is introduced to the open-ended SIW, forming the radiation mechanism. On either side of the radiating element are extensions of the vias, improving isolation between adjacent elements in an array, thereby resulting in greater CP purity and reduced side lobe levels.

To demonstrate the antenna's ability to radiate with circular polarization at a wide range of azimuth steering directions, three 4x1 arrays are manufactured for three fixed beam directions (0°, 15° and 30°), using the splitter described previously, and vertical posts within the appropriate SIWs to generate the delays required for those fixes beams. Fig. 9 presents the measured normalized right-handed CP (RHCP) and left-handed CP (LHCP) radiation patterns of the 4x1

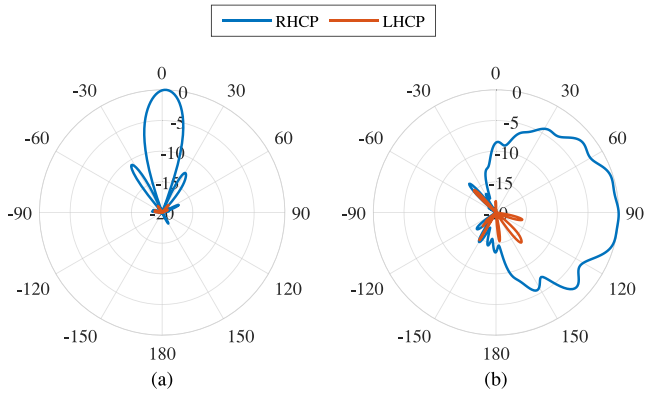

FIGURE 9. Measured normalized RHCP (co-polarization) and LHCP (cross-polarization) radiation patterns of the 0° azimuth steering fixed beam array at 27.9 GHz. (a) Azimuth plane. (b) Elevation plane.

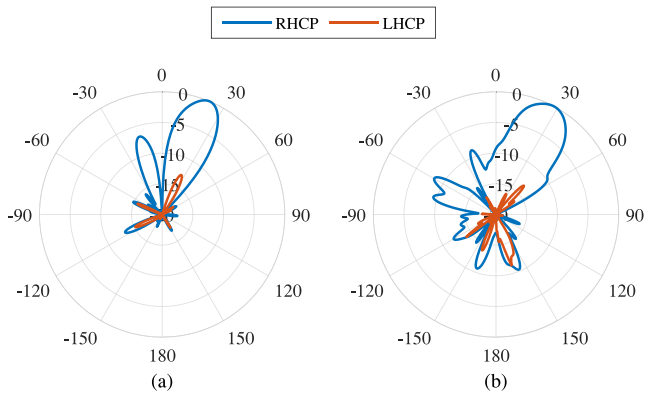

FIGURE 10. Measured normalized RHCP (co-polarization) and LHCP (cross-polarization) radiation patterns, in the azimuth plane, of the fixed beam arrays at 27.9 GHz. (a) 15° array. (b) 30° array.

array with fixed 0° azimuth steering in azimuth and elevation, while Fig. 10 presents the measured normalized RHCP and LHCP radiation patterns for the 4x1 arrays for fixed beam directions of 15° and 30°, as measured and presented in [27]. The radiation patterns demonstrate that the polarizer and antenna designs meet our requirements for CP and wide enough azimuth range. The arrays' efficiency was measured to be 69% [27]. These presented arrays are, however, not yet suitable for practical applications since they, each, radiate in only one specific azimuth direction. Using the SIW phase shifter presented earlier, rather than fixed vertical posts within the SIW would make the beam steerable.

D. COUPLERS

As mentioned in the introduction and to be discussed in greater detail in Section II, compactness is achieved through the stacking of the different blocks in a multi-layered system. Thus, it is important to design couplers to transfer power from the splitter on a 1.8-mm-thick substrate layer to the phase shifter on a 0.5-mm-thick substrate, and also from the phase shifter to the input of the polarizer on a 1.8-mm-thick substrate. Specifically, two types of couplers are required: forward couplers where the SIWs on the two layers flow in one direction, and reverse couplers when the fields in the SIWs propagate in opposite directions. The stack consists of three substrate layers with metal layers between each substrate layer and at the top and bottom of the stack. The layouts of the two couplers are shown in Fig. 11. Some metal layers are not shown in the isometric views for clarity. Slots couple energy from one SIW to the other while inductive posts in substrate 1 allow for better matching. Dimensions are provided in Tables 4 and 5. The SIW widths are chosen to match the SIW widths of the blocks being coupled: splitter & RTPS for the reverse coupler, and RTPS & polarizer for the forward coupler.

As seen by the simulation results in Fig. 12, an impedance BW of 9.9% and an IL of 0.7 dB are achieved by the forward coupler while an impedance BW of 9.3% and an IL of 0.5 dB are observed for the reverse coupler.

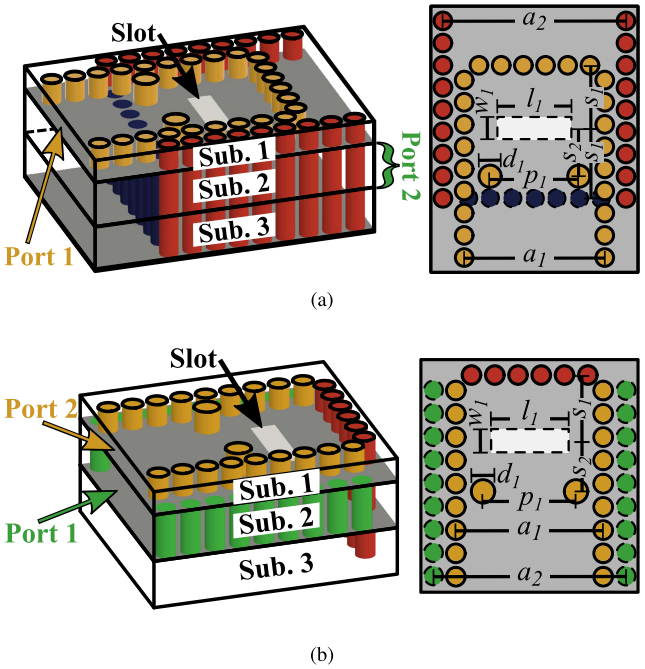

FIGURE 11. Layout of the couplers for the beamsteering system. Isometric views and the metal between substrates 1 and 2 are shown. (a) Forward coupler. (b) Reverse coupler.

TABLE 4. Dimensions of the forward coupler for the beamsteering system.

Parameter	a_1	a_2	l_1	w_1	s_1	s_2	p_1	d_1
Value (mm)	4.4	4.5	3.3	0.2	0.5	1.0	2.7	0.4

TABLE 5. Dimensions of the reverse coupler for the beamsteering system.

Parameter	a_1	a_2	l_1	w_1	s_1	s_2	p_1	d_1
Value (mm)	4.4	5.3	3.3	0.2	0.5	1.0	2.8	0.4

IV. MEASUREMENT AND DISCUSSION

The beamsteering system is manufactured and assembled in order to characterize its performance, as shown in

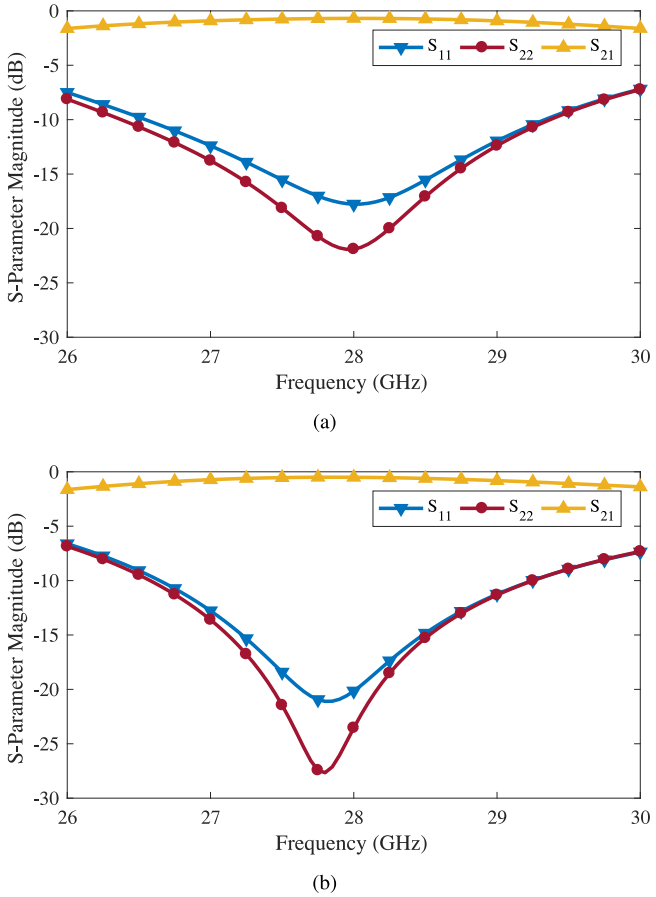

FIGURE 12. Simulated S-Parameter magnitudes of the couplers. (a) Forward coupler. (b) Reverse coupler.

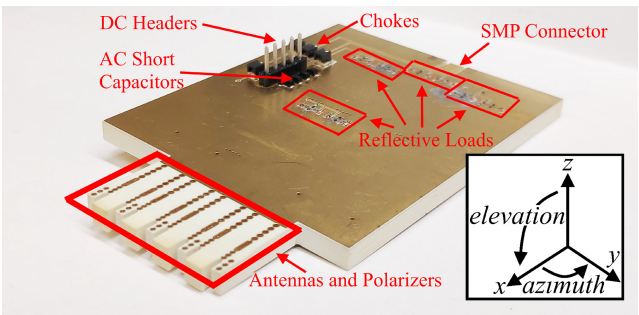

FIGURE 13. Photograph of the end-fire, CP, SIW 4 × 1 beamsteering system prototype.

Fig. 13. Five header pins are included, with four being individually used for the control voltages of the four phase shifters, while the fifth being for DC ground. Additionally, RF chokes and decoupling capacitors are also present at the headers to reduce any noise from the power supplies.

A. MEASUREMENT

Before the system's radiation is characterized, its input impedance matching is measured. It is shown in Fig. 14 that the simulated impedance BW is 9.1%. A measured

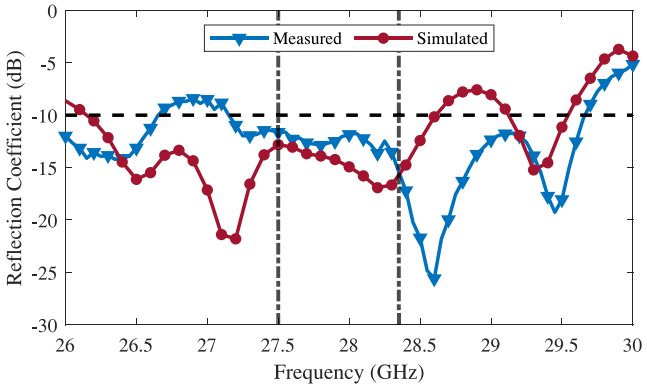

FIGURE 14. Measured and simulated impedance matching of the beamsteering system. The vertical lines indicate the 850 MHz 5G band at 28 GHz.

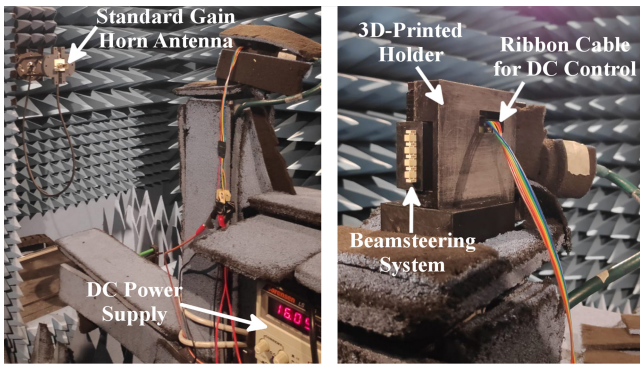

FIGURE 15. Anechoic chamber setup to measure the radiation performance of the beamsteering system. (a) Overview showing the probe, the beamsteering system, and a DC power supply. (b) Closeup of the beamsteering system setup in the elevation orientation.

TABLE 6. Beamsteering system control voltages for desired beam directions.

θ_s (°)	V_1 (V)	V_2 (V)	V_3 (V)	V_4 (V)
0	16.0	16.0	16.0	16.0
17	16.0	10.8	6.5	0.8
35	10.3	0.0	16.0	6.5

impedance matching BW of 8.9% is achieved, sufficiently covering our intended band of operation of 27.5 GHz to 28.35 GHz.

The system's gain and AR are measured in an NSI-MI anechoic chamber with a 3D-printed holder for proper alignment and stability, as shown in Fig. 15. Variable DC power supplies are used to control the phase shifters to achieve the desired beam directions. We conducted measurements for the following azimuth steering angles: 0°, 17°, and 35°. Using (1) and the measured phase shifter voltage-phase curve from Fig. 5, we obtained the required control voltages for the four phase shifters for the desired beam directions at 28 GHz. The control voltages, with subscripts 1 to 4 for elements 1 to 4, are listed in Table 6.

Fig. 16 presents the measured and simulated normalized right-handed CP (RHCP) and left-handed CP (LHCP)

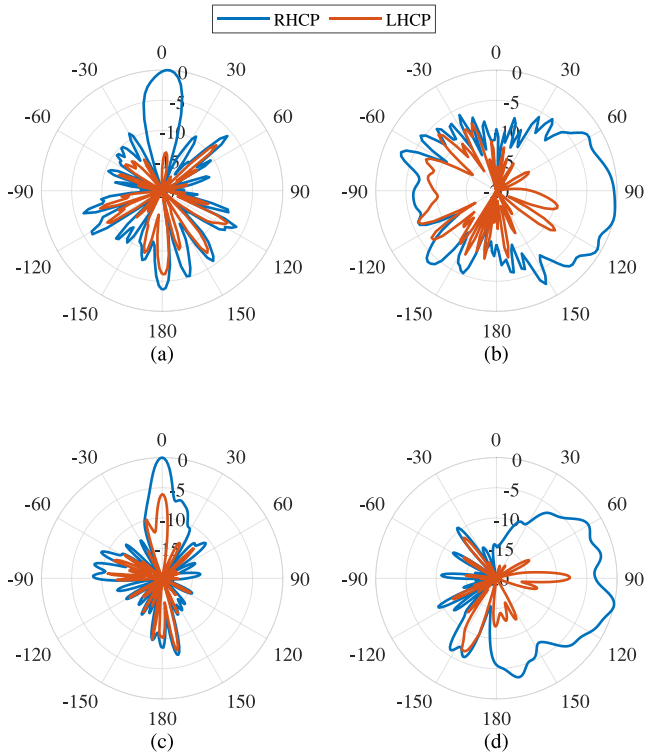

FIGURE 16. Normalized RHCP (co-polarization) and LHCP (cross-polarization) radiation patterns of the proposed beamsteering system with 0° azimuth steering at 27.9 GHz. (a) Azimuth plane (simulated). (b) Elevation plane (simulated). (c) Azimuth plane (measured). (d) Elevation plane (measured).

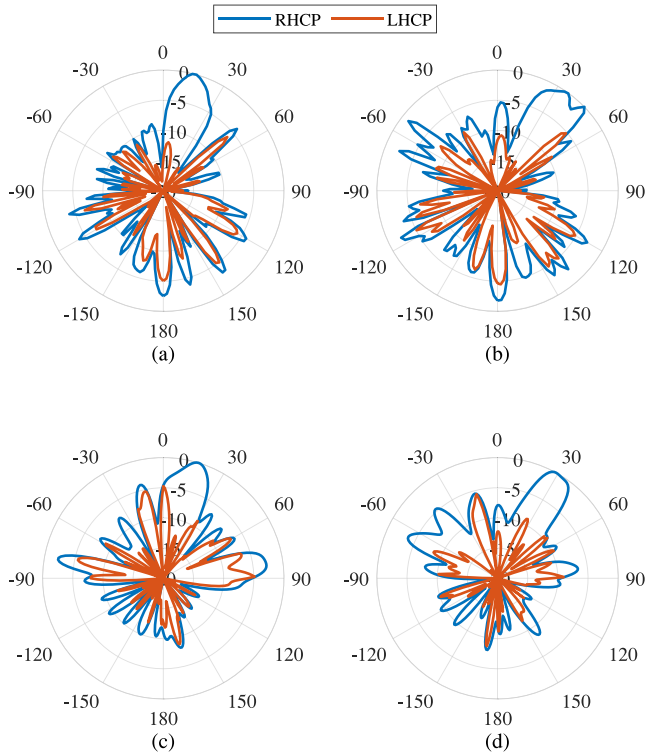

FIGURE 17. Normalized RHCP (co-polarization) and LHCP (cross-polarization) radiation patterns, in the azimuth plane, of the proposed beamsteering system when steered beyond 0° at 27.9 GHz. Steering angle: (a) 17° (simulated). (b) 35° (simulated). (c) 17° (measured). (d) 35° (measured).

radiation patterns of the proposed beamsteering array in azimuth and elevation at 0° azimuth steering. The simulated and measured radiation patterns in the elevation plane are similar. The measurement demonstrates ripples, which can be attributed to radiation from the GCPW-to-SIW transition slots. An elevation half-power beamwidth (HPBW) of 72° is measured, which is 10° smaller than the simulated one. The simulated and measured RHCP peaks are both detected 14° below the azimuth plane. The manufactured prototype demonstrated a front-to-back (F/B) ratio of 10.9 dB compared to the simulated F/B ratio of 6.3 dB. Similar peaks in the LHCP radiation patterns are observed in the forward direction thus reducing the AR at those angles. However, as shown by Fig. 16(b), the angles of maximum gain in LHCP and RHCP measured elevation patterns do not coincide. Besides the spikes in LHCP gain at those narrow angles, the simulated and measured elevation 3 dB AR beamwidths are both a little under 120°. An azimuth HPBW of 10° is measured, which is half that expected from simulations. This difference could be attributed, to some degree, to the ripples in the elevation plane which are in return likely resultant from reflections from the measurement setup and radiation from the GCPW-to-SIW slots. Not illustrated in the normalized plot, but also measured, is the maximum measured gain of 1.9 dBi. This lower gain can be easily compensated with a low-cost power or low-noise amplifier for transmit or receive paths, respectively.

The capability to electronically steer the beam in azimuth is illustrated by the normalized radiation patterns in Fig. 17. Figs. 17(a) and (c) demonstrate azimuth steering to 16° in simulation, and 17° in measurement. A HPBW of 22° is achieved in both measurement and simulation. Within the RHCP main beam, the LHCP levels are low for both results. There are slight differences however. The first side lobe in measurement is at −14° at −4.1 dB, while in simulation the first side lobe is at 50° at −3.9 dB. Furthermore, more side lobes of around −2.5 dB are seen at ±80° in measurement, while in simulation more side lobes appear at ±120° at −4.1 dB. While different, both measured and simulated side lobe levels can be attributed to the difference in the gain for different phase shift settings, i.e., the array is not a uniform linear array. Figs. 17(b) and (d) demonstrate the radiation patterns for the intended azimuth steering to 35°. The realized steering in azimuth is 32° in measurement and 36° in simulation. An azimuth HPBW of 19° is measured. Besides the reduced AR performance resulting from the peaks in LHCP at 27° and 38°, the measured 3 dB AR beamwidth adequately covers the radiation HPBW. This is similarly observed in simulation, albeit with smaller LHCP peaks and thus better AR. A grating lobe of −3.7 dB is detected in measurement at −66° implying that the beamsteering system could be steered further in azimuth before interference due to side lobe levels of −3 dB.

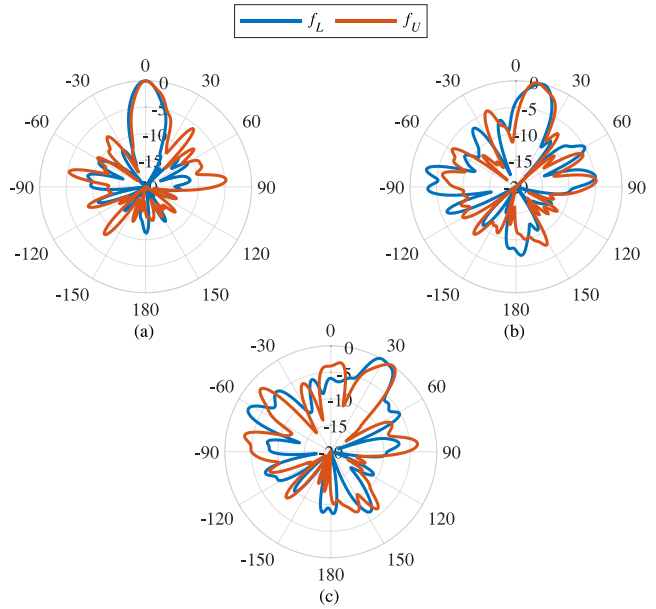

FIGURE 18. Measured normalized RHCP (co-polarization) radiation patterns in the azimuth plane at the lower ($f_L = 27.8$ GHz) and upper ($f_U = 28.2$ GHz) edges of a probable 400 MHz user channel band. Steering angle: (a) 0°. (b) 17°. (c) 35°.

While the phase shifters' non-flat delays versus frequency could theoretically result in different beam directions on user channel band edges, that is unlikely since the array will operate within 5G channel band sizes of 50 MHz to 400 MHz [33]. When operated in smaller user BWs, the phase shifters' control voltages can be appropriately chosen for the center of those channel bands, rather than for the center frequency of the total BW of the system. This is demonstrated, in Fig. 18, by the measured azimuth radiation patterns at 27.8 GHz and 28.2 GHz. Despite being at the edges of the maximum user channel BW of 400 MHz, the worst-case difference in beam direction is only 3° (15% of the HPBW), indicating that the phase shifters' performance is sufficiently flat.

Fig. 19 demonstrates that the AR performance over frequency of measurements and simulations are identical. For 0° steering, the 3 dB AR BW is measured to be from 27.7 GHz to 28.3 GHz, compared to 27.7 GHz to 28.7 GHz in simulation. The measured 3 dB AR BW for 17° steering is from 27.2 GHz to 28.3 GHz, while in simulation it is from 27.1 GHz to 28.6 GHz. Finally, for 35°, the measured and simulated 3 dB AR BWs are both from 27.6 GHz to 28.0 GHz. From 28.0 GHz to 28.35 GHz, at 35° steering, the AR is still observed to be better than 5.7 dB in measurement and better than 4.8 dB in simulation. The beamsteering system thus demonstrates reasonable AR performance within the intended 5G band of operation of 27.5 GHz to 28.35 GHz. The larger AR values at the edges of the band are attributed to the phase error versus frequency. However, this is not a big concern given real-life implementation would see relatively smaller channel BWs as discussed in the previous paragraph.

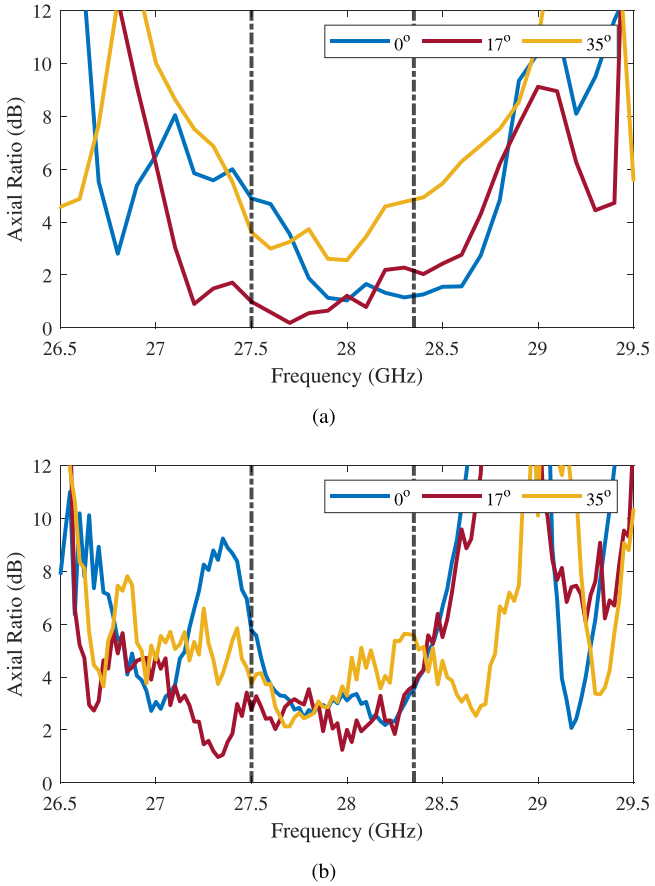

FIGURE 19. AR of the proposed beamsteering system in frequency for several azimuth steering angles. The vertical lines indicate the 850 MHz 5G band at 28 GHz. (a) Measured. (b) Simulated.

B. COMPARISON TO LITERATURE

In order to compare our proposed beamsteering system with other recent beamsteering solutions in literature, their performances and characteristics are tabulated in Table 7. While the systems in [21] and [22] are capable of achieving greater than ±30° steering in azimuth, they do not produce CP patterns, are large, and require additional space for a mechanism to select the beams, rendering them less useful for 5G mobile applications. The systems in [23] and [24] address the shortcomings of the previous two designs in terms of polarization by creating CP patterns with AR of better than 3 dB up to ±30° and ±25°, respectively. They still suffer from large footprints that are made even larger through the need of a mechanism to switch between beams. The structure presented in [25] is tiny in size although it still requires additional structures to switch beams. While it has a wide azimuth steering range of ±90°, it lacks the ability to generate CP radiation. Additionally, it demonstrated wide azimuth beamwidths of at least 45° and as large as 75° in its various steering states making it likely to result in interference. Finally, it is not as simple to implement in mobile terminals since it is not monolithic (requiring an additional dielectric block). A common limitation of the systems in [21], [22], [23], [24], [25] are their switched

TABLE 7. Comparison of different SIW beamsteering systems.

	This Work	[18]	[21]	[23]	[24]	[25]	[26]
Structure	**4×1 SIW, RTPS, Septum Polarizer, Dielectric Lens**	8×1 SIW, Butler Matrix, ME-Dipole	15×1 SIW, Rotman Lens, Leaky-Wave	4×1 SIW, Butler Matrix, Septum Polarizer, Dielectric Lens	4×1 SIW, Butler Matrix, Septum Polarizer, Open-Ended	3×1 SIW, Switched Parasitics, Monopoles	4×1 SIW, RTPS, Patches
Size $L \times W \times H$ ($\lambda_o{}^3$)	**7.6×4.1×0.38**	19×10.9×0.44	10.4×8×0.13	17.5×5×0.38	8.6×3.8×0.7	1.2×1.6×0.23	3.3×2.6×0.18
f_c (GHz)	**28**	60	24	37.5	60	28	5.5
BW (%)	**8.9**	16.4	4.2	29.3	7.8	>25	16.1
3 dB Gain Variation Steering Range	$>\pm$**35°**	$>\pm$35°	$\pm$33°	$\pm$38°	$\pm$37°	$>\pm$90°	$\pm$45°
3 dB AR Steering Range	$\pm$**35°**	N/A	N/A	$\pm$30°	$\pm$25°	N/A	N/A
CP	✓			✓	✓		
Compact	✓					✓	✓
Continuous Steering	✓						✓
Edge-Radiating	✓	✓		✓	✓	✓	
Integrated Control Lines	✓	N/A	N/A	N/A	N/A		
mmWave	✓	✓	✓	✓	✓	✓	
Multi-Layer, Single Stack PCB Only	✓	✓	✓	✓	✓		
Single RF Feed	✓					✓	✓

N/A: Not Applicable

Compact: Both length and width are $\leq 10\lambda$, and height is $\leq 0.5\lambda$

beam nature which means only pre-defined beam patterns are possible, thus resulting in more interference with other users, and reducing gain and signal-to-noise ratio due to limited beam direction options. That is not the case for the continuous beamsteering system in [26], which is also presented in a small package with a wide gain steering range of $\pm 45°$. It, however, does not generate CP patterns and is not monolithic, requiring screws and mounts. Furthermore, the structure requires active elements on its underside as well, rendering integration into mobile terminals less straightforward. Finally, its performance is not necessarily translatable to our higher frequency of operation where varactors become lossier. Our proposed system's size and BW fall within the range of those of the other presented designs. It achieves similar azimuth gain steering range to most of the other designs ($\pm 35°$) while, unlike all the other designs, also providing 3 dB AR within that range and being capable of continuous steering. The simple fabrication and the lack of the need for additional steering mechanisms mean that our system can be easily integrated within a typical mobile handset.

V. CONCLUSION

In this paper, a compact, CP, end-fire 4×1 continuous beamsteering system in SIW is designed for 5G mobile terminals. The array addresses the challenges of fitting beamsteering and circular polarization functionality in the limited space in a mobile terminal, and of ensuring that the design can be consistently manufactured and easily integrated within standard mobile terminal technology. The designed system seamlessly integrates antennas, polarizers, variable phase shifters, and a feeding network in a compact multi-layered PCB ($7.6 \times 4.1 \times 0.38\lambda_o^3$). The beamsteering system's compactness is achieved through the stacking of the phase shifters on top of the feeding network, and through the use of forward and reverse couplers. Ease of

integration is resultant from the multi-layer, single stack PCB design, integrated control lines and single RF feed. The measurements illustrate a continuous CP beamsteering range of $\pm 35°$ and an impedance BW of 8.9% at 28 GHz. Given its performance, size, and ease of manufacture and integration, the proposed beamsteering array is a good candidate for 5G mmWave continuous beamsteering in mobile terminals. This array, when introduced on each edge of a mobile terminal, can be used alongside planar antenna arrays to ensure spherical coverage around the terminal, thereby ensuring communication link integrity at any orientation and rotation.

ACKNOWLEDGMENT

The authors would like to thank Dr. Ashwin Iyer for providing access to the anechoic chamber, and Braden Smyth and Stuart Barth for assistance with performing measurements.

Last, but not least, this work would have not been possible without the generous samples of dielectric substrates, capacitors and inductors provided by Rogers Corporation, Passive Plus Inc., and CoilCraft, respectively.

REFERENCES

[1] F. Boccardi, R. W. Heath, A. Lozano, T. L. Marzetta, and P. Popovski, "Five disruptive technology directions for 5G," *IEEE Commun. Mag.*, vol. 52, no. 2, pp. 74–80, Feb. 2014.

[2] T. S. Rappaport et al., "Millimeter wave mobile communications for 5G cellular: It will work!" *IEEE Access*, vol. 1, pp. 335–349, 2013.

[3] W. Roh et al., "Millimeter-wave beamforming as an enabling technology for 5G cellular communications: Theoretical feasibility and prototype results," *IEEE Commun. Mag.*, vol. 52, no. 2, pp. 106–113, Feb. 2014.

[4] A. Goudarzi, A. Gharaati, M. M. Honari, R. Mirzavand, and P. Mousavi, "A steerable beam patch antenna for millimeter-wave band application," in *Proc. IEEE Int. Symp. Antennas Propag. North American Radio Sci. Meet*, 2020, pp. 591–592.

[5] B. Mazdouri, M. M. Honari, R. Mirzavand, and P. Mousavi, "Gain enhancement of curvy spoof surface plasmon Polariton antenna with controllable bandwidth for 5G applications," in *Proc. IEEE Int. Symp. Antennas Propag. North American Radio Sci. Meet*, 2020, pp. 1641–1642.

[6] Federal Communications Commission, "Use of spectrum bands above 24 GHz for mobile radio services; proposed rules," *Fed. Reg.*, vol. 81, no. 8, pp. 1802–1849, Jan. 2016. [Online]. Available: https://www.gpo.gov/fdsys/pkg/FR-2016-01-13/pdf/2015-31852.pdf

[7] H. Friis, "A note on a simple transmission formula," *Proc. IRE*, vol. 34, no. 5, pp. 254–256, May 1946.

[8] U. Ullah, M. Al-Hasan, S. Koziel, and I. B. Mabrouk, "Series-slot-fed circularly polarized multiple-input–multiple-output antenna array enabling circular Polarization diversity for 5G 28 GHz indoor applications," *IEEE Trans. Antennas Propag.*, vol. 69, no. 9, pp. 5607–5616, Sep. 2021.

[9] Y. Yin and K. Wu, "Combined planar end-fire circularly Polarized antenna using unidirectional dielectric radiator and thin substrate integrated waveguide feeder," *IEEE Trans. Antennas Propag.*, vol. 69, no. 11, pp. 7298–7307, Nov. 2021.

[10] H. Uchimura, T. Takenoshita, and M. Fujii, "Development of a laminated waveguide," *IEEE Trans. Microw. Theory Techn.*, vol. 46, no. 12, pp. 2438–2443, Dec. 1998.

[11] Y. Cassivi, L. Perregrini, P. Arcioni, M. Bressan, K. Wu, and G. Conciauro, "Dispersion characteristics of substrate integrated rectangular waveguide," *IEEE Microw. Wireless Compon. Lett.*, vol. 12, no. 9, pp. 333–335, Sep. 2002.

[12] F. Xu and K. Wu, "Guided-wave and leakage characteristics of substrate integrated waveguide," *IEEE Trans. Microw. Theory Techn.*, vol. 53, no. 1, pp. 66–73, Jan. 2005.

[13] F. M. Monavar, S. Shamsinejad, R. Mirzavand, J. Melzer, and P. Mousavi, "Beam-steering SIW leaky-wave subarray with flat-topped footprint for 5G applications," *IEEE Trans. Antennas Propag.*, vol. 65, no. 3, pp. 1108–1120, Mar. 2017.

[14] A. Ghalib, M. S. Sharawi, R. Mittra, H. Attia, and A. Shammim, "Collocated MIMO travelling wave SIW slot array antennas for millimetre waves," *IET Microw. Antennas Propag.*, vol. 15, no. 8, pp. 815–826, Apr. 2021.

[15] W. Hong, K. H. Baek, Y. Lee, Y. Kim, and S. T. Ko, "Study and prototyping of practically large-scale mmWave antenna systems for 5G cellular devices," *IEEE Commun. Mag.*, vol. 52, no. 9, pp. 63–69, Sep. 2014.

[16] Y. Cao, Y. Cai, L. Wang, Z. Qian, and L. Zhu, "A review of substrate integrated waveguide end-fire antennas," *IEEE Access*, vol. 6, pp. 66243–66253, 2018.

[17] W. El-Halwagy, R. Mirzavand, J. Melzer, M. Hossain, and P. Mousavi, "Investigation of wideband substrate-integrated vertically-polarized electric dipole antenna and arrays for mm-wave 5G mobile devices," *IEEE Access*, vol. 6, pp. 2145–2157, 2018.

[18] A. Li, K. Luk, and Y. Li, "A dual linearly polarized end-fire antenna array for the 5G applications," *IEEE Access*, vol. 6, pp. 78276–78285, 2018.

[19] X. Ruan and C. H. Chan, "An Endfire circularly polarized complementary antenna array for 5G applications," *IEEE Trans. Antennas Propag.*, vol. 68, no. 1, pp. 266–274, Jan. 2020.

[20] K. Al-Amoodi, M. M. Honari, R. Mirzavand, J. Melzer, D. G. Elliott, and P. Mousavi, "Circularly-polarised end-fire antenna and arrays for 5G millimetre-wave beam-steering systems," *IET Microw. Antennas Propag.*, vol. 14, no. 9, pp. 980–987, 2020.

[21] K. Tekkouk, M. Ettorre, L. L. Coq, and R. Sauleau, "Multibeam SIW slotted waveguide antenna system fed by a compact dual-layer Rotman lens," *IEEE Trans. Antennas Propag.*, vol. 64, no. 2, pp. 504–514, Feb. 2016.

[22] Y. Li and K. M. Luk, "A multibeam end-fire magnetoelectric dipole antenna array for millimeter-wave applications," *IEEE Trans. Antennas Propag.*, vol. 64, no. 7, pp. 2894–2904, Jul. 2016.

[23] Q. Wu, J. Hirokawa, J. Yin, C. Yu, H. Wang, and W. Hong, "Millimeter-wave multibeam endfire dual-circularly polarized antenna array for 5G wireless applications," *IEEE Trans. Antennas Propag.*, vol. 66, no. 9, pp. 4930–4935, Sep. 2018.

[24] X. Cheng et al., "A compact multi-beam end-fire circularly polarized septum antenna array for millimeter-wave applications," *IEEE Access*, vol. 6, pp. 62784–62792, 2018.

[25] S. Zhang, I. Syrytsin, and G. F. Pedersen, "Compact beam-steerable antenna array with two passive parasitic elements for 5G mobile terminals at 28 GHz," *IEEE Trans. Antennas Propag.*, vol. 66, no. 10, pp. 5193–5203, Oct. 2018.

[26] Y. Ji, L. Ge, J. Wang, Q. Chen, W. Wu, and Y. Li, "Reconfigurable phased-array antenna using continuously tunable substrate integrated waveguide phase shifter," *IEEE Trans. Antennas Propag.*, vol. 67, no. 11, pp. 6894–6908, Nov. 2019.

[27] K. Al-Amoodi, R. Mirzavand, M. M. Honari, J. Melzer, D. G. Elliott, and P. Mousavi, "A compact substrate integrated waveguide notched-septum Polarizer for 5G mobile devices," *IEEE Antennas Wireless Propag. Lett.*, vol. 19, no. 12, pp. 2517–2521, Dec. 2020.

[28] A. Sebak and L. Shafai, "The sidelobe performance of a phased array antenna with fine incremental scan steps," in *Proc. Dig. Antennas Propag. Soc. Int. Symp.*, 1989, pp. 698–701.

[29] Y. Ding and K. Wu, "Varactor-tuned substrate integrated waveguide phase shifter," in *Proc. IEEE MTT-S Int. Microw. Symp. (MTT)*, 2011, pp. 1–4.

[30] Y. Ding and K. Wu, "SIW varactor-tuned phase shifter and phase modulator," in *Proc. IEEE MTT-S Int. Microw. Symp. Dig. (MTT)*, 2012, pp. 1–3.

[31] W. M. Abdel-Wahab and S. Safavi-Naeini, "A simple circuit model for planar waveguide power splitters used for millimeter-wave beam forming network," in *Proc. IEEE Int. Symp. Antennas Propag. (APSURSI)*, 2011, pp. 8–11.

[32] R. Y. Fang, C. F. Liu, and C. L. Wang, "Compact and broadband CB-CPW-to-SIW transition using stepped-impedance resonator with 90°-bent slot," *IEEE Trans. Compon. Packag. Manuf. Technol.*, vol. 3, no. 2, pp. 247–252, Feb. 2013.

[33] *5G; NR; User Equipment (UE) Radio Transmission and Reception; Part 2: Range 2 Standalone, Version 15.4 Release 15*, ETSI, Sophia Antipolis, France, Apr. 2019. [Online]. Available: https://www.etsi.org/deliver/etsi_ts/138100_138199/13810102/15.04.00_60/ts_13810102v150400p.pdf

KHALED AL-AMOODI (Member, IEEE) received the B.Sc. degree in electrical engineering with a specialization in nanoengineering from the University of Alberta, Edmonton, AB, Canada, in 2013, where he is currently pursuing the Ph.D. degree in computer engineering, under the supervision of Prof. D. G. Elliott.

He is currently working with LinkedIn Corporation, Sunnyvale, CA, USA, as a Software Engineer. He has filed a U.S. patent and has coauthored several academic publications. His research interests include mmWave circuits and phased-array antennas for mobile communication applications.

Mr. Al-Amoodi has been awarded several scholarships during his Ph.D. program, including the Queen Elizabeth II Graduate Scholarship.

RASHID MIRZAVAND (Senior Member, IEEE) received the B.Sc. degree in electrical engineering from the Isfahan University of Technology, Isfahan, Iran, in 2004, and the M.Sc. and Ph.D. degrees in electrical engineering from the Amirkabir University of Technology (Tehran Polytechnic), Tehran, Iran, in 2007 and 2011, respectively.

He is currently an Assistant Professor with the Department of Electrical and Computer Engineering, University of Alberta, Edmonton, AB, Canada, where he leads the Intelligent Wireless Technology Group. He is also an Adjunct Fellow with the Faculty of Engineering and IT, University of Technology Sydney, Australia. He has three granted and eight filled U.S. patents and is the coauthor of more than 100 journal and 70 conference papers. His major research interests include, but are not limited to, RF/microwave/mm-wave circuits, sensors, reconfigurable intelligent surfaces and antennas, numerical methods, and measurement systems.

Dr. Mirzavand received various awards, such as the Best AUT M.Sc. Researcher in 2007, the Best AUT Ph.D. Researcher in 2011, the Best MICT National Researcher in 2013, the National Elite Foundation Young Professor Grant in 2014, the AITF Elite PDF in 2015, the Honorable CMC Industrial Collaboration in 2017, the TEC Edmonton Innovation in 2019, the CMC Industrial Collaboration in 2021 as the Supervisor, the UofA Innovation in 2021, and three UofA Innovation in 2022. He serves as the Specialty Chief Editor of Frontiers in the Internet of Things (IoT Enabling Technologies Section). He is a Registered Member of the Association of Professional Engineers and Geoscientists of Alberta.

MOHAMMAD MAHDI HONARI (Senior Member, IEEE) received the B.Sc. degree in electrical engineering from the Ferdowsi University of Mashhad, Mashhad, Iran, in 2009, the M.Sc. degree in electrical engineering from the Amirkabir University of Technology, Tehran, Iran, in 2012, and the Ph.D. degree in electrical engineering from the University of Alberta, Edmonton, AB, Canada, in 2019.

He was a Research Scholar with the Radiation Laboratory, University of Michigan at Ann Arbor, Ann Arbor, MI, USA, in 2018. He was also a Postdoctoral Fellow with the University of Alberta in 2019. He was a Research Associate with the University of Wisconsin–Madison, Madison, WI, USA, from August 2020 to September 2022. He is currently working with Kymeta Corporation, Redmond, WA, USA, as a Staff Antenna Engineer. His research interests include phased-array antennas, leaky-wave structures, metamaterial, and batteryless radio frequency identification sensors.

Dr. Honari received several awards, including the GSA Professional Development Award in 2015, the AITF Scholarship from 2015 to 2017, the Sadler Graduate Scholarship in 2016 and 2018, the GSA Research Assistantship Award, the Martha Piper Award, the Honorable CMC Industrial Collaboration Award in 2017, the TEC Edmonton Innovation Award in 2017 and 2019, and the NSERC Postdoctoral Fellowship during his Ph.D. and Postdoctoral programs.

JORDAN MELZER (Member, IEEE) received the B.A.Sc. degree in engineering science from the University of Toronto, and the M.S.E.E. and Ph.D. degrees in communications from the University of Southern California. He currently serves as a Network Architect with TELUS Communications, Canada. Prior to joining TELUS, he co-developed TrellisWare Technology's F-LDPC error control code product and was part of an IP RAN Research Team with Nortel Networks. He has coauthored several dozen academic and industry publications. He is an Associate Technical Editor of *IEEE Communications Magazine*.

DUNCAN G. ELLIOTT (Senior Member, IEEE) received the B.A.Sc. degree in engineering science and the master's and Doctoral degrees in electrical and computer engineering from the University of Toronto.

He is a Professor with the Department of Electrical and Computer Engineering, University of Alberta, Edmonton, Canada. Previously, he has worked with the Nortel in data communications, with MOSAID Technologies as a DRAM Designer, and with IBM Microelectronics as a Contractor in application-specific memory design. He has been granted 17 U.S. patents. His research interests include RF and communications circuits, high resolution radar, merged microfluidic-microelectronic systems, information processing architectures, uncrewed aircraft systems, and satellite design.

Prof. Elliott was the 2001 winner of the Colton Medal in microelectronics for his work on Computational RAM, which has been commercialized. His group has designed and built four satellites that have been launched, producing a wealth of open-source designs. He has served on multiple national committees guiding future use and regulation of uncrewed aircraft. He is a member of the IEEE Solid State Circuits, Circuits and Systems, Antennas and Propagation, Computer, and Aerospace and Electronic Systems Societies.

PEDRAM MOUSAVI (Senior Member, IEEE) received the B.Sc. (Hons.) degree in telecommunication engineering from the Iran University of Science and Technology, Tehran, Iran, in 1995, and the M.Sc. and Ph.D. degrees in electrical engineering from the University of Manitoba, Winnipeg, MB, Canada, in 1997 and 2001, respectively.

He was a Professor with the Department of Mechanical Engineering and the NSERC-AI Industrial Research Chair of Intelligent Integrated Sensors and Antennas with the University of Alberta, Edmonton, AB, Canada. He had over eighteen years of entrepreneurial academic experience with start-up companies from the University of Waterloo, Waterloo, ON, USA, and the University of Alberta. He founded Intelwaves Technologies as a spin-off with the University of Waterloo. He was a Co-Founder of WiDyne Technologies, SenZIoT Technologies, and Anteligen Technologies spin-offs with the University of Alberta. His mission was to foster a strong collaboration between industry and academia and stimulate more industry relevant research in wireless technologies. His research conducted through his industrial chair program allowed information and communications technology innovations to be applied to the areas of intelligent integrated sensors and antennas to improve the productivity of the oil-energy sector and to sustain its growth. His research interests were in the areas of advanced intelligent antenna, microwave and millimetre-waves circuits and systems, 5G phased array antennas, UWB radar systems, 3-D printing electronics, wearable antennas, and zero-power IoT. He had more than 250 refereed journal and conference articles and several patents in this field.